\$ SUPER

Contents lists available at ScienceDirect

# Atmospheric Research

journal homepage: www.elsevier.com/locate/atmosres



# Characteristics of upward-connecting-leader current leading to attachment in downward negative cloud-to-ground lightning strokes

Amitabh Nag a,b,\*, Kenneth L. Cummins b,c, Mathieu N. Plaisir b, Robert G. Brown d,e, Jennifer G. Wilson d, David E. Crawford d, R. Carl Noggle b, Hamid K. Rassoul b

- <sup>a</sup> Los Alamos National Laboratory, Los Alamos, NM, USA
- <sup>b</sup> Florida Institute of Technology, Melbourne, FL, USA
- University of Arizona, Tucson, AZ, USA
- <sup>d</sup> NASA Kennedy Space Center, FL, USA
- e University of Central Florida, FL, USA

#### ARTICLE INFO

#### Keywords: Cloud-to-ground lightning

Upward positive leaders Upward connecting leaders Attachment processes Current measurements Charge transferred to ground

#### ABSTRACT

We analyzed currents associated with upward connecting leaders (UCLs) initiated from the Kennedy Space Center Industrial Area Tower in two negative cloud-to-ground strokes that struck the tower. One stroke was also recorded using a high-speed video camera located 760 m from the KSC IAT. The NLDN-reported peak currents for the two strokes were - 31.7 and - 98.5 kA. During the UCL development phase the current waveforms exhibited a monotonically (quasi-exponentially) increasing "background" current overlaid with 10-µs scale pulses with a median amplitude of 51.1 A. The UCL current durations for the two strokes were 1039 and 449 µs, respectively. During the pre-attachment processes (UCL and slow front) the total negative charge effectively transferred to ground were 70.2 and 55 mC, respectively. For the stroke captured on high-speed video, the average line-chargedensity for the 109-m long UCL was found to be 0.5 mC/m. The average UCL 2-D speed was  $2.4 \times 10^5$  m/s, and it was observed to accelerate toward the downward leader prior to attachment. We observed that UCL-pulse amplitudes are larger, background currents are higher, and interpulse intervals are shorter at later times during UCLs, which can be attributed to the intensification of the local electric field due to the approaching downward negative leader. The median positive charge injected into the UCL by a pulse was 297 μC. The UCL associated with the higher peak-current stroke produced the highest injected pulse-charge values about three times sooner during its development, likely due to the 2-2.7 times faster average downward leader vertical speeds.

#### 1. Introduction

The Industrial Area Tower (IAT) at the Kennedy Space Center (KSC) is a 91.5-m tall tower (with grounded guy-wires attaching to different heights on the tower) located in a region with flat ground with a lightning flash density in the range of 8 to 12 flashes/sq. km/year (Nag et al., 2021). A lightning current measurement system was installed at the top of this tower to measure currents associated with natural downward lightning processes including upward connecting and unconnected leaders as well as first return-stroke slow-fronts and fast-transitions. Nag et al. (2021) provide a detailed analysis of currents of eight upward unconnected leaders (UULs) initiated from the IAT. UUL-currents consisted of faster (total durations of the order of 10  $\mu$ s) impulses overlaid

on slower (millisecond-scale) "background" current. From the perspective of charge transferred to ground, UULs can be considered to be a bipolar lightning phenomenon. Nag et al. (2021) defined the time-period between the inception of a UUL's current and the current-polarity reversal (which occurs at the time of the nearby return stroke) as its development phase and the time-period following the current-polarity reversal as its collapse phase. All UULs studied by Nag et al. (2021) initially transferred negative charge to ground (median of 6.4 mC over a median time-period of 789  $\mu$ s) followed by an effective transfer of positive charge to ground (median of 4.7 mC over a median time-period of 388  $\mu$ s).

Tall (effective height > 150 m or so) towers/objects tend to initiate upward lightning, often triggered by nearby positive cloud-to-ground

<sup>\*</sup> Corresponding author at: Los Alamos National Laboratory, Los Alamos, NM, USA. *E-mail addresses*: anag@fit.edu, anag@lanl.gov (A. Nag).

lightning (e.g., Warner et al., 2012; Yuan et al., 2017; Yuan et al., 2021). As a result, measurements of currents of downward first strokes in natural lightning attaching to instrumented tall objects are relatively rare (e.g., Berger et al., 1975; Visacro et al., 2004, 2010, 2012; Takami and Okabe, 2007; Miki et al., 2019; Chen et al., 2022). Such measurements can provide important insights into the characteristics of return-stroke current pulses which are important for lightning protection system design, lightning locating system validation, and power systems analyses (e.g., CIGRE TB 549, 2013, Rakov and Uman, 2003, Ch. 18; Fuchs et al., 1998; Narita et al., 2000; Nag et al., 2015; Schulz and Nag, 2020). Detailed measurements and characterization of currents associated with the upward connecting leader (UCL) in natural downward negative lightning remain scarce (e.g., Visacro et al., 2010; Visacro et al., 2017a; Qiu et al., 2019). Understanding the characteristics of UCLs is important for deciphering the details of the attachment processes that follow the UCL in downward cloud-to-ground lightning (e.g., Tran and Rakov, 2017; Nag et al., 2023) as well as for lightning protection and safety. Visacro et al. (2017a) examined the characteristics of UCLs in negative cloud-to-ground lightning at the Morro do Cachimbo Station (MCS) near Belo Horizonte, Brazil using current, electric field, and high-speed video camera measurements. UCL currents consist of millisecond-scale "background" current overlaid with faster current pulses, as is the case for UUL current signatures. However, for UCLs the current keeps rapidly (quasi-exponentially) increasing with time all the way up to the return-stroke peak, and unlike UUL-currents, there is no current-polarity reversal during UCLs. Visacro et al. (2017a) estimated the two-dimensional (2-D) arithmetic mean propagation speed for three UCLs to be 0.6, 1, and  $1.6 \times 10^5$  m/s.

Conventionally, especially for the purposes of modeling (e.g., Nag and Rakov, 2016; Rakov and Uman, 1998), the return-stroke pulse is defined to begin following the attachment of the upward and downward leaders. The initial rising portion of the return-stroke current and their associated electric field waveforms have two separate phases called the slow front and fast transition (Weidman and Krider, 1978; Nag et al., 2012). The slow-front current in first strokes has often been attributed to the presence of a UCL (e.g., Rakov and Uman, 2003, p. 144) or been associated with the common streamer zone formed prior to the attachment of the upward and downward leaders (e.g., Cooray et al., 2004). In return-stroke electric radiation field waveforms (measured at distances of several tens of kilometers from a stroke's location), the slow front appears as the initial (typically concave-shaped) deflection of the field from the zero or background value prior to the stroke and occurs soon after the last leader step (e.g., Nag et al., 2012). Sometimes, a leader-step pulse (likely associated with stepping in a downward leader branch, rather than in the main leader channel which attaches to the upward leader) is overlaid on the slow front field change. This relatively-slowly rising portion of the field waveform is about 2-8 µs in duration and constitutes as much as roughly half the return-stroke peak field amplitude (Weidman and Krider, 1978). Recent time-synchronized ultra-highspeed video camera and electromagnetic field/channel-base current measurements of downward negative natural lightning strokes (Nag et al., 2023; Plaisir et al., 2023) show that the appearance of the common streamer zone is marked by a rapid increase in field/current associated with the slow front. The fast transition follows the slow front and is an abrupt transition to peak, which according to Weidman and Krider (1978, 1980), has a 10-to-90% risetime of 0.1–0.2  $\mu s$  or less for first strokes when the field propagation is over seawater.

In this paper, we examine in detail the characteristics of measured current-waveforms of UCLs leading to attachment and return-stroke pulses for two downward negative strokes that struck the KSC-IAT. We also examine high-speed video camera data for one stroke and discuss the line-charge-density characteristics of the UCL.

# 2. Measurement system and data

The measurement system at the IAT is described in detail by Nag

et al. (2021). It consists of a shunt and a Rogowski coil near the base of a 6.2-m tall mast and Franklin rod installed at the top of the 91.5-m tall tower. Current from the base of the Franklin rod was brought by a downconductor to the current measurement box at the tower-top that contains the shunt and Rogowski coil. The current was measured in four separate channels, three from the shunt followed by electronic amplifiers, and one from the Rogowski coil followed by an integrator, resulting in broadband (DC -10 MHz for shunt and 0.05 Hz -10 MHz for Rogowski coil) current measurements in the range of 1.73 A to 200 kA. The root mean square (RMS) noise floor for a bandwidth upper-limit of 1 MHz was 0.64 A. Data in all channels were transmitted via fiber optic links from the tower-top to its base where they were digitized using a 12bit oscilloscope at a rate of 25 MHz (sampling interval of 40 ns). The record-length was 2 s with a 750-ms pre-trigger. All data were GPS timestamped to allow correlation with other datasets. In this study, we examined current waveforms of two UCLs leading to attachments to the tower on August 9, 2018 (stroke 080918) and July 26, 2019 (stroke 072619). Fig. 1 shows the return-stroke current waveforms recorded by three of our measurement channels (two shunt and the Rogowski coil) for the stroke occurring on August 9, 2018. The shunt channel 3 (saturating at  $\pm 120$  kA) was not operational for this case. Note that in this paper the polarity of the current indicates the polarity of charge being effectively transferred to ground. As summarized in Table 1, the U.S. National Lightning Detection Network (NLDN) and the Mesoscale Eastern Range Lightning Information System (MERLIN) (Nag et al., 2021; Hill et al., 2016; Roeder and Saul, 2017) geolocated stroke 080918 at distances of 360 and 200 m from the tower, respectively, and stroke 072619 at distances of 230 and 43 m, respectively. Stroke 080918 appeared to be the last stroke of a four-stroke negative cloud-to-ground flash that followed a new channel to ground and terminated on the tower. Stroke 072619 was the first stroke of a six-stroke negative cloudto-ground flash. Only the first stroke terminated on the tower. Note that this stroke, which had an NLDN-reported peak current of 98.5 kA, damaged our Rogowski coil. Additionally, the first two shunt channels were saturated (by design) prior to the return-stroke current peak and the third channel appeared to be affected by relatively large-amplitude high-frequency noise immediately preceding the return-stroke peak. As a result, the peak current for this stroke could not be accurately measured. Based on the waveform behavior prior to and during recovery from saturation, we estimate the peak current to have been in the range of 100-120 kA.

We analyzed the time-evolution of UCL currents (both the background current and the microsecond-scale current pulses) in a manner similar to the analyses of the UUL currents reported by Nag et al. (2021) to facilitate intercomparison. In order to obtain reliable estimates of computed charge transferred to ground during various (low-current and high-current) stages of the strokes, we digitally integrated our most sensitive current measurement channel available until its saturation, at which point we used the next most sensitive measurement channel available.

A Phantom Miro high-speed video camera, located at 760 m from the tower, recorded stroke 072619 at 10,000 frames per second (98.46  $\mu s$  exposure time, 1.54  $\mu s$  deadtime) with a 50 mm lens. The pixel resolution was 0.313 m/pixel. The attachment of the downward and upward leaders occurred within the field-of-view of the camera. The sensitivity was set such that the return-stroke frame was not overexposed. The camera record was used to determine the 2-D length of the upward leader for this stroke. Finally, we used very high frequency (VHF) data from the KSC Lightning Mapping Array (LMA) to determine average speeds for the downward negative leaders of both strokes in our dataset.

# 3. Characteristics of upward connecting and downward leaders

We examined in detail the characteristics of the upward connecting and downward leaders in each of the two strokes in our dataset using measured currents and video camera records. A summary of the UCL-

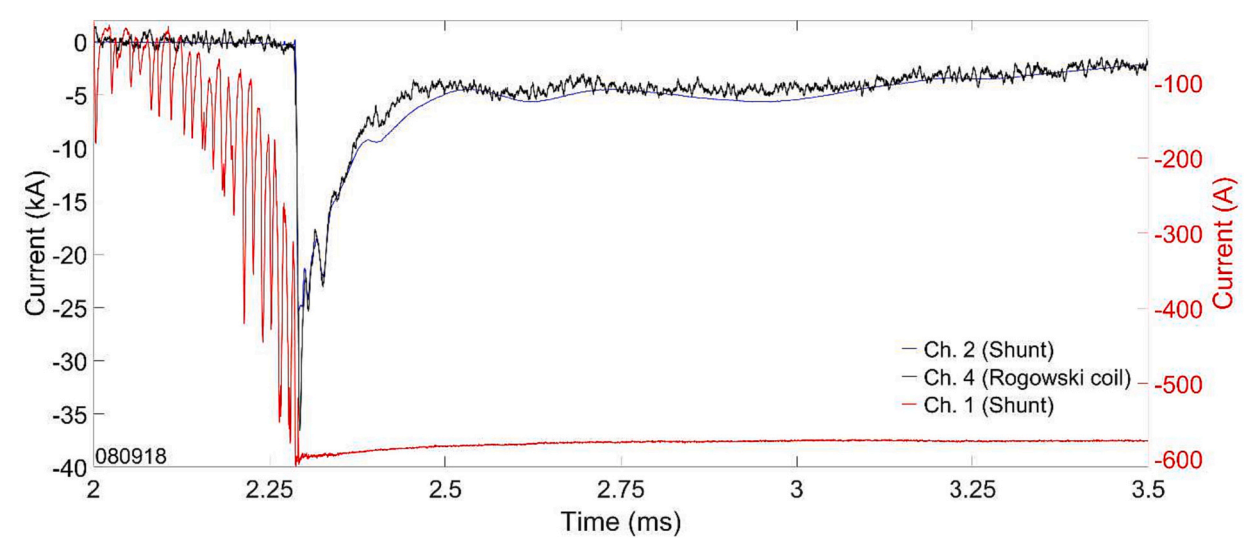


Fig. 1. Return-stroke current waveforms recorded by three of our measurement channels for the stroke occurring on August 9, 2018, shown on a 1.5-ms timescale. The polarity of the current waveform indicates the polarity of charge being effectively transferred to ground. The current in channels 1 and 2 (red and blue waveforms, respectively), both measured by the shunt, saturated at about -600 A and -25 kA, respectively. The current in channel 4 (black waveform) was measured by the Rogowski coil, which had an upper measurement-limit of about 200 kA. The vertical axis for channel 1 is shown on the right and that for channels 2 and 4 is on the left. Current pulses associated with the UCL are seen in the waveform recorded in channel 1.

Table 1
Characteristics of the two strokes measured at the KSC IAT and reported by the NLDN and MERLIN.

Stroke	Stroke type	NLDN repor	rts	MERLIN reports		
ID		Distance from tower (m)	RS peak current (kA)	Distance from tower (m)	RS peak current (kA)	
080918	Last stroke via new channel to ground of a four- stroke negative flash	360	-31.6	200	-31.6	
072619	First stroke of a six-stroke negative flash; only stroke that terminated on the tower	230	-98.5	43	-87.4	

characteristics is presented in Table 2.

# 3.1. Overall UCL, slow front, and fast transition characteristics – duration, charge transferred, and propagation speed

We defined the duration of the UCL development phase as the time-interval between the inception of current in the most sensitive current measurement channel (with a lower-measurement-limit of 0.64 A) and the beginning of the slow front. We considered the slow front in the current waveform (see Figs. 2b and 3b, respectively, for strokes 080918 and 072619) to occur at the end of the monotonically (quasi-exponentially) increasing "background" UCL current overlaid with microsecond-scale pulses (see Figs. 2a and 3a). For stroke 080918 (Fig. 2b), we could see a relatively sharp change in the rate of UCL-current increase that could be defined as the onset of the slow front. On the other hand, for stroke 072619 (Fig. 3b), the rate of increase in the UCL current leading to the slow front was more gradual, i.e., the rate of change in current was somewhat less pronounced (than in stroke 080918) between the slow front portion of the current waveform and the UCL current preceding it.

Nevertheless, a change in slope of current at the beginning of the slow front (labeled in Figs. 2b and 3b) could be discerned for both strokes. Next, in order to define the end of the slow front and the beginning of the fast transition, we considered the highest-slope portion of return stroke pulse immediately preceding the peak; the fast transition was marked by a clear increase in the slope of the current relative to the preceding slow-front current.

The UCL durations for strokes 080918 and 072619 were 1039 and 449 µs, respectively, during which 51.1 and 43 mC of negative charge, respectively, was effectively transferred to ground (see Figs. 2c and 3c). The current increased in magnitude from zero to 1.5 kA and 3.6 kA at the end of the UCL stage (labeled in Figs. 2b and 3b) for the two strokes, respectively, which were 4.1% and 3.7% of the respective return-stroke peak current. Note that for stroke 072619, we used the NLDN-reported peak current to calculate the percentage, as we did not measure the return-stroke peak current (and charge transfer) for this stroke (as discussed in Section 2). The slow-front durations (which occur after the change in current-slope at the end of the UCL-stage) for strokes 080918 and 072619 were 2.2 and 1.8  $\mu s$ , respectively. During the slow front, the current increased by 11.8 and 7~kA to reach amplitudes of 13.3 and 10.6kA for the two strokes, respectively, which were 37 and 10.8% of the respective return-stroke peak current. 19.1 and 12 mC of negative charge was effectively transferred to ground during the slow front stage for the two strokes, respectively.

The fast transition 10-to-90% duration for stroke 080918 was 1.84  $\mu s$ , and the rate of rise of current during this phase was 11.1 kA/ $\mu s$ . The return-stroke peak current was -36.6 kA. We computed the charge transferred over a 6.03-ms time-interval between the inception of the fast transition in the return-stroke current waveform and when the return-stroke continuing current decayed to zero; 8.52 C of negative charge was effectively transferred to ground during this stage. During the UCL, slow front, and return-stroke stages combined, 8.59 C of negative charge was effectively transferred to ground by stroke 080918. The parameters reported in this paragraph could not be measured for stroke 072619, due to the reasons discussed in Section 2.

Fig. 4 shows two successive video-camera frames captured while the UCL and the return stroke were in progress for stroke 072619 recorded by our high-speed video camera. The tip of the UCL and the tower (top of our Franklin rod) is labeled in Fig. 4a. The attachment point of the upward and downward leaders, inferred using the direction of branching

Characteristics of the UCLs and return strokes (RSs) in the two strokes in our dataset determined from measured currents and video camera records.

		333	(2017) 2011/2012 111												
Stroke ID	On	UCL current characteristics	cteristics		Slow front current characteristics	rent characteris	stics	Total pre- attachment		Fast transition current characteristics	RS c charac	RS current characteristics	UCL came	UCL camera-derived characteristics	racteristics
	Duration, µS	Duration, Current at Charge us UCL end", transfers kA (% of during L RS peak) mC	Charge transferred during UCL, mC	Duration, µS	Duration, Current at slow-front end', kA (% of RS peak)	Current increase during slow front	Charge transferred during slow front, mC	charge transfer, mC	10-to-90% fast transition duration, µs	Fast transition maximum rate of rise, kA/µs	Peak (current t (kA) (	Charge ransfer,	UCL 2-D UCL length, avera m speed	UCL average speed, m/ s	UCL charge per unit length, mC/m
080918 1039	1039	1.5 (4.1) 51.1	51.1	2.2	-13.3(37) $-10.6$	11.8	19.1	70.2	1.84	11.1	$-36.6$ $-8.52^{d}$	-8.52 <sup>d</sup>	1		1
072619	449	3.6 (3.7°) 43	43	1.8	(10.8 <sup>b</sup> )	^	12	55	ı	ı	ı	ı	109	$2.4 \times 10^{\circ}$	0.5

a Current is zero at the start of the UCL.

Calculated using the NLDN-estimated peak current of -98.5 kA.

Computed over a 6.03-ms time-interval between the fast transition start-time and RS continuing current end-time. Slow front starts when the UCL ends.

Computed using the ratio of the sum of charge transferred during UCL and slow-front stages and the UCL 2-D length observed in the video camera frame in Fig. 4b.

extending from the UCL, is labeled in Fig. 4b. The attachment point was at an altitude of 182.6 m above ground level (AGL). We can estimate the speed of the UCL based on its 2-D (on the plane of the video-camera frame) length and time measured either using the camera inter-frame interval or the duration of the UCL current waveform. The 2-D length of the UCL was estimated using the length of the path (shown in Fig. 4b with a thin red line overlaid on the UCL) along the channel. They were 46.1 m (see Section 4.1 for further discussion) and 109 m, in Fig. 4a and b, respectively. Assuming that the 46.1-m UCL extension occurred entirely during the first frame (Fig. 4a), we computed (using the 100-µs inter-frame interval) an average 2-D upward extension speed for the UCL of 4.6  $\times$  10<sup>5</sup> m/s. This extension speed is likely an overestimate as it is probable that the 46.1-m upward extension of the UCL from the towertop occurred over a longer period of time (than one frame-duration) but the UCL was not sufficiently visibly luminous during early-times to be recorded by our video camera. For the next frame (Fig. 4b), we computed an extension speed of  $6.3 \times 10^5$  m/s. Note that the extension speed for this frame should be treated as underestimate, as we are unable to determine at which point in the 100-us inter-frame interval the return-stroke onset occurred. Additionally, there appears to be a significant component of the UCL-length that was perpendicular to the video-camera frame, resulting in the 2-D length being an underestimate of the actual (3-D) one. The average UCL speed, assuming that the 109-m UCL-extension occurred during the 200-µs combined duration of the two frames, was  $5.5 \times 10^5$  m/s. On the other hand, the duration of current from UCL-start to the end of the slow front (at which point, presumably, the downward and upward leaders merge/attach, see Section 4.1 for further discussion) for this stroke was 451 µs. If we consider the life cycle of the UCL to be lasting this entire duration rather than just when a luminous hot channel was visible in our video camera frames, an average speed of  $2.4 \times 10^5$  m/s is obtained. Using the total charge transferred during the pre-attachment phase (from the inception of the UCL-current to the end to the slow front) of 55 mC, the average linecharge-density for the 109-m long positively-charged UCL was found to be 0.5 mC/m.

### 3.2. Downard leader propagation speed

For stroke 072619, the 2-D length-extension of the downward leader during the 100-µs inter-frame interval between its tip labeled in Fig. 4a and the attachment point in Fig. 4b was 14.5 m, yielding a 2-D downward leader extension speed of  $1.45 \times 10^5$  m/s just prior to attachment. This speed is likely an underestimate due to the same reasons discussed in the previous paragraph.

Fig. 5 shows the scatter plot of the KSC LMA VHF source altitudes versus time relative to the NLDN-reported ground-strike time for the two strokes. We obtained an estimate of the downward leader vertical speed using these data. For stroke 080918, the average vertical speeds were  $1.8 \times 10^5$  m/s between the 5.5 and 2.75 km and  $2.3 \times 10^5$  m/s below 2.75 km AGL. The average vertical speeds for stroke 072619 were 3.6  $\times$  $10^5$  m/s and  $6.3 \times 10^5$  m/s, respectively, for the two altitude ranges.

# 3.3. Characteristics of microsecond-scale UCL pulses

As shown in Figs. 2a and 3a, UCL-currents consist of faster (total durations of the order of 10 µs) impulses overlaid on a slower (millisecond-scale) "background" current. We examined in detail the characteristics of the microsecond-scale current pulses that occurred during the development of the two UCLs in our dataset. These pulses result in the injection of positive charge into the upward leaders effectively transferring negative charge to ground. Table 3 shows the characteristics of these pulses in the two UCLs and Fig. 6a-f show histograms of the characteristics. The median pulse total duration, full-width at half maximum (FWHM), background-to-peak risetime, and 10-to-90% risetimes for 79 pulses in the two UCLs were 11.6, 4, 3.4, and 1.9  $\mu s,$ respectively. The background-to-peak pulse amplitude, which is the

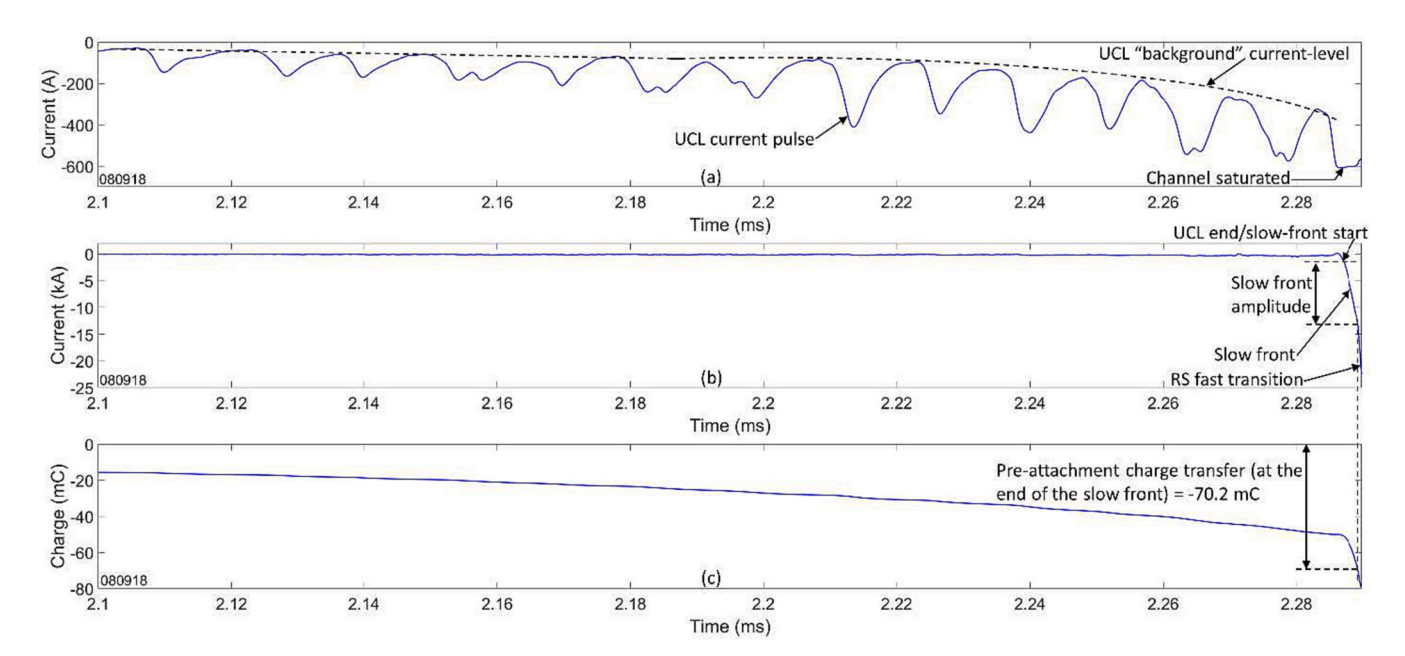


Fig. 2. Current waveforms for stroke 080918 measured using the (a) 600-A and (b) 25-kA shunt channels shown on a 190-μs timescale. The dotted black line in (a) indicates the estimated "background" current level during the UCL stage on which UCL current pulses (one is labeled in (a)) are overlaid. The UCL stage ends when the slow front starts in the current waveform as labeled in (b). The end of the slow front is marked by the inception of the fast transition. (c) The charge transfer was computed by appropriately integrating the measured current waveforms. Note that the inception of the UCL current occurred prior to the beginning of this time-window.

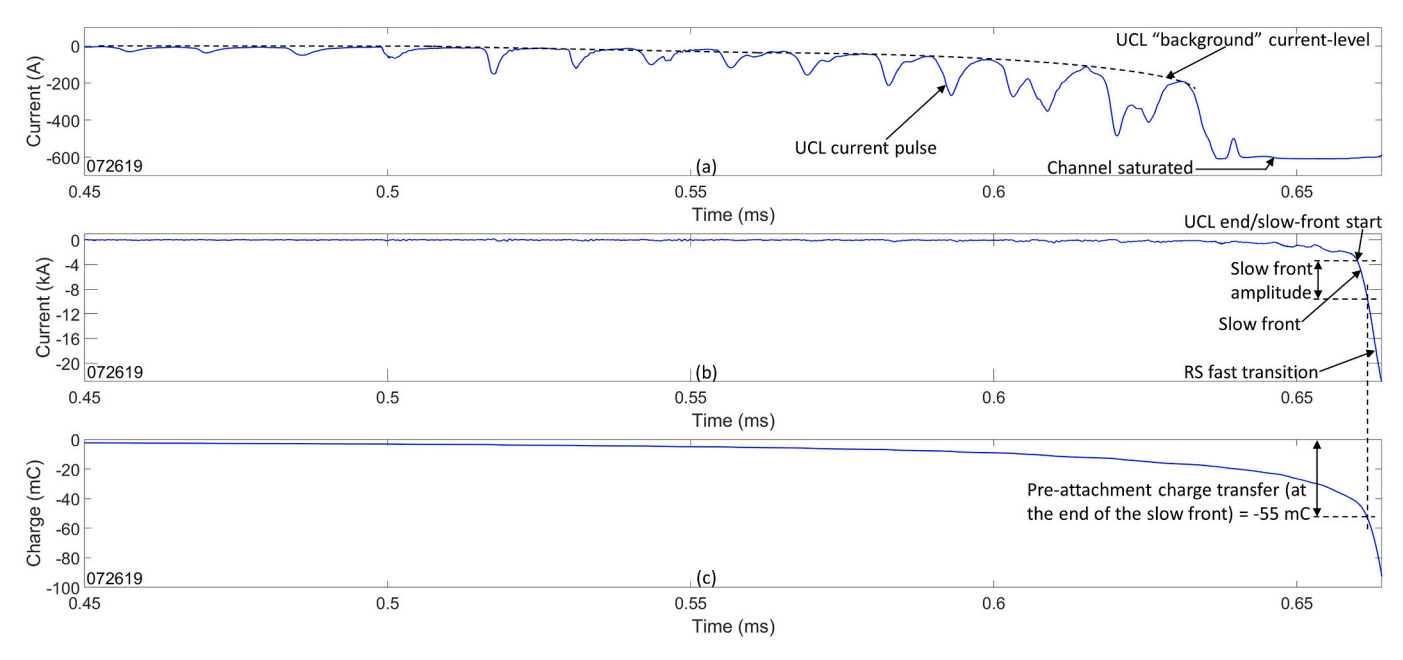


Fig. 3. Current waveforms for stroke 072619 measured using the (a) 600-A and (b) 25-kA shunt channels shown on a 214-µs timescale. The dotted black line in (a) indicates the estimated "background" current level during the UCL stage on which UCL current pulses (one is labeled in (a)) are overlaid. The UCL stage ends when the slow front starts in the current waveform as labeled in (b). The end of the slow front is marked by the inception of the fast transition. (c) The charge transfer was computed by appropriately integrating the measured current waveforms. Note that the inception of the UCL current occurred prior to the beginning of this time-window.

pulse amplitude relative to the background current-level at the start of each pulse (rather than the zero current-level) ranged from 6 to 376 A, with the median being 51.1 A. Interpulse intervals (N=77) ranged from 10.3 to 33.7  $\mu$ s, with the median being 16.4  $\mu$ s. The negative charge injected by each pulse (between its start and end times) into the developing UCL ranged from 30.1 to 4467  $\mu$ C, with the median being 297  $\mu$ C. The histogram of the magnitude of the injected pulse charge is shown in Fig. 7a. For both our UCLs, the magnitude of the injected pulse

charge increased geometrically for pulses occurring later in the UCL, as can be seen from Fig. 7b, which shows the scatter plot of the pulse-charge magnitude versus time from first-pulse peak.

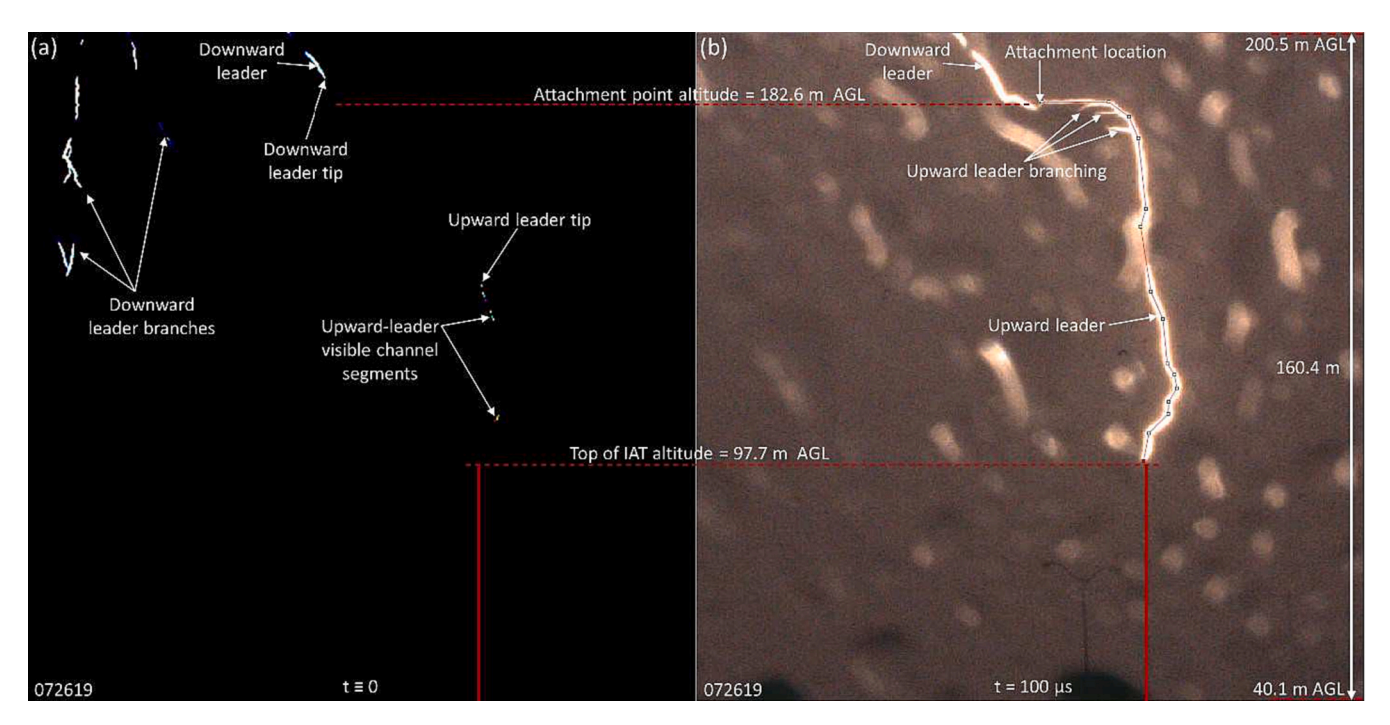
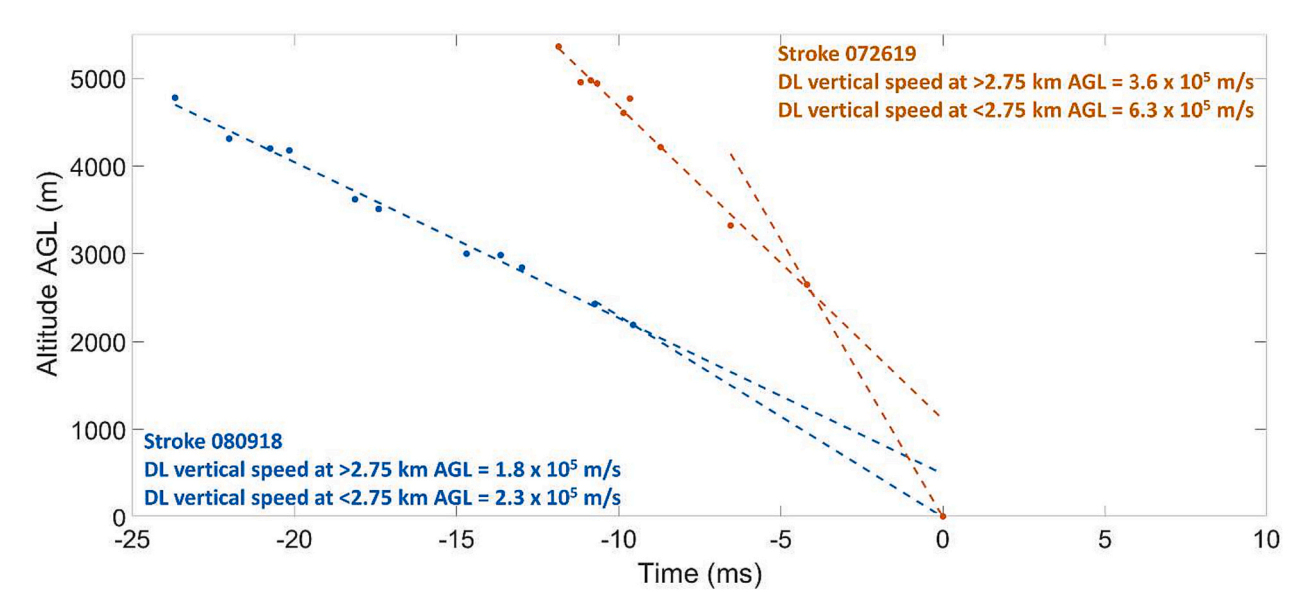


Fig. 4. Two successive frames showing stroke 072619 at the IAT recorded by our high-speed video camera at 10,000 fps. Each frame had a 98.46-µs exposure-time. The IAT, the top of which was at 97.7 m AGL, is indicated by the red vertical line in both frames. (a) This frame shows segments of the UCL and downward leader as they approached each other. The tips of the two leaders are labeled. The image was enhanced to make visible sections of the UCL channel that were not emitting brightly in the visible range. (b) This frame shows the return stroke in progress soon after the attachment of the UCL and downward leader. The sensitivity of our camera was set such that the return-stroke frame was not overexposed. The attachment point and UCL branches are labeled in this image. The attachment point was at an altitude of 182.6 m AGL. The thin red line drawn along the UCL indicates the 2-D path whose length was used to estimate the UCL 2-D length.



**Fig. 5.** Scatter plot of the KSC LMA VHF-source altitudes AGL versus time relative to the NLDN-reported ground-strike time (t = 0) for stroke 080918 (in blue) and 072619 (in orange). The dashed lines indicate the slopes, i.e., the average downward leader (DL) vertical speeds for altitudes between 5.5 and 2.75 km and below 2.75 km for each stroke.

# 4. Discussion

#### 4.1. On leader characteristics and cloud-to-ground attachment processes

Our overall average 2-D UCL speed of  $2.4 \times 10^5$  m/s for the 109-m long UCL072619 was comparable to (but greater than) the average 2-D speeds of  $0.6 \times 10^5$  to  $1.6 \times 10^5$  m/s reported by Visacro et al. (2017a) for 52–83 m long UCLs at the Morro do Cachimbo Station in

Brazil, as well as the speed of  $1.4 \times 10^5$  m/s reported by Saba et al. (2022) for a roughly 11-m long segment of UCL from a tall (about 80 m AGL, Saba, personal communication, Saba et al., 2023) building in Brazil. For lightning striking trees in Gainesville, Florida, Tran and Rakov (2017) reported 2-D speeds ranging from  $1.8 \times 10^5$  to  $6.0 \times 10^5$  m/s for 11–25 m long UCLs (in virgin air prior to the formation of the common streamer zone), with an arithmetic mean (AM) of  $3.4 \times 10^5$  m/s, which is similar to our UCL's average speed. Also, for a 400 m long UCL

Table 3
Summary of characteristics of microsecond-scale current pulses in the two UCLs. Note that these pulses injected positive charge into the UCLs, therefore, effectively transferring negative charge to ground.

Flash ID	Parameters	Total duration, μs	Full-width at half maximum, µs	Background-to-peak risetime, μs	10-to-90% risetime, μs	Background-to-peak pulse amplitude, A	Interpulse interval, μs	Pulse charge magnitude, μC
UCL080918	Median Sample size Range	12.8 N = 56 4.1-22.3	4.6 N = 56 1.1–11.8	3.7 N = 56 0.8-9.9	2.0 N = 56 0.4-9.7	45.7 N = 56 6-335	17.7 $N = 55$ $11-33.7$	336 N = 56 30.1-4467
UCL072619	Median Sample size Range	8.7 N = 23 5.6–15.3	2.5 $N = 23$ $1.3-8.1$	$\begin{array}{c} 2.1 \\ N = 23 \\ 0.7  8.3 \end{array}$	1.1 $N = 23$ $0.4-7$	66.3 N = 23 18.2-376	15.1  N = 22  10.3-22.6	201 N = 23 52-3779
All	Median Sample size Range	11.6  N = 79  4.1-22.3	4.0 N = 79 1.1–11.8	3.4 N = 79 0.7-9.9	1.9 N = 79 0.4-9.7	51.1 N = 79 6-376	$16.4 \\ N = 77 \\ 10.3-33.7$	297 N = 79 30.1–4467

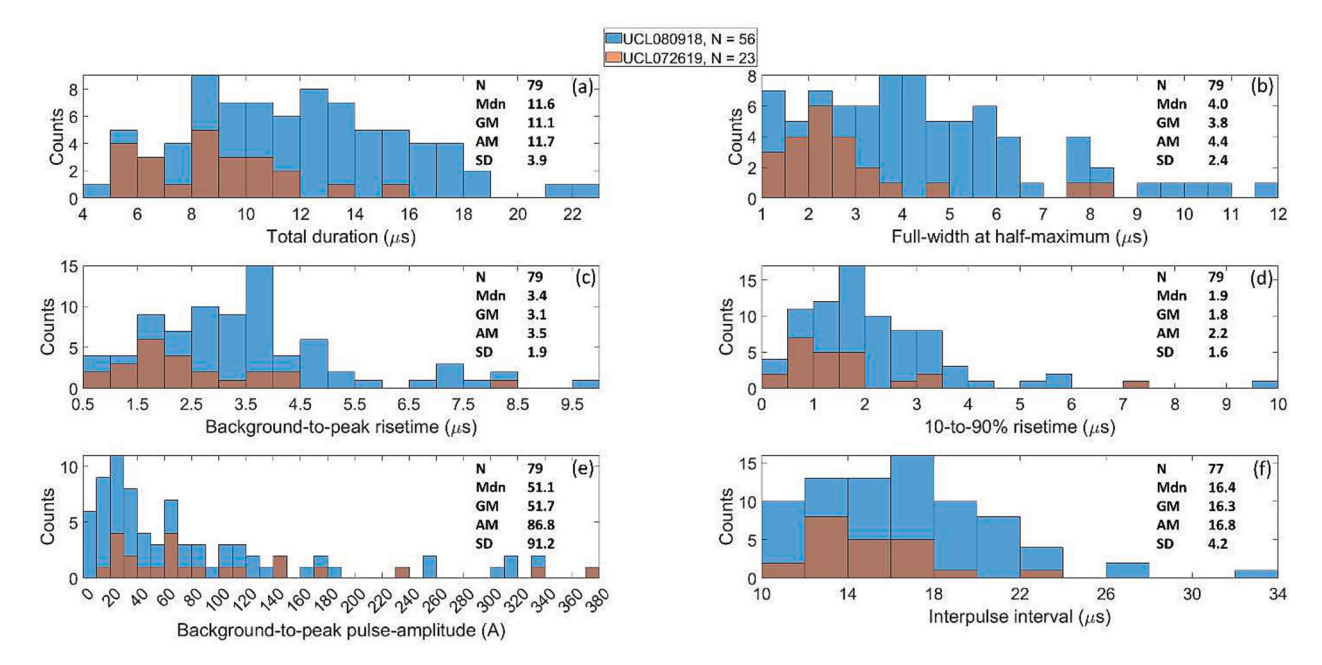
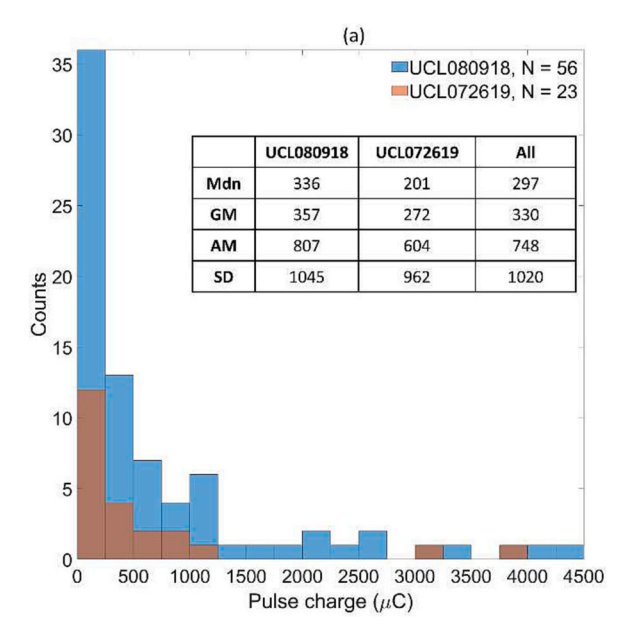


Fig. 6. Histograms showing the (a) total duration, (b) full-width at half-maximum, (c) background-to-peak risetime, (d) 10-to-90% risetime, (e) absolute background-to-peak pulse amplitude, and (f) interpulse interval for current pulses occurring during the two UCLs in our dataset (56 pulses in UCL080918 are shown in blue bars and 23 pulses in UCL072619 are shown in brown bars). Statistics shown are sample size (N), median (Mdn), geometric mean (GM), arithmetic mean (AM), and standard deviation (SD). The corresponding maximum and minimum values are shown in Table 3.

initiated from a 440 m tall building, Lu et al. (2013) reported an AM speed of  $4.2 \times 10^5$  m/s, which is comparable to our UCL speed. Our observation indicated that the UCL speed increased from 4.6  $\times$   $10^5$ (which is very likely an overestimate, see Section 3.1) to  $6.3 \times 10^5$  m/s (likely an underestimate) as the UCL extended upward to attach to the downward leader. This observation of the UCL's upward acceleration is consistent with those by Visacro et al. and Tran and Rakov. Also, for two long (about 180 and 230 m) UCLs initiated from tall (>100 m) towers, Warner (2010) reported 2-D speeds increasing from 2.6  $\times$  10<sup>4</sup> to 2.8  $\times$  $10^5$  m/s and from  $8.4\times10^4$  to  $3.7\times10^5$  m/s. Next, we discuss a potential source of error/uncertainty in our estimate of UCL speed. Note that the UCL is faintly luminous in the frame shown in Fig. 4a. In upward positive leaders, sometimes the luminosity of the lower section of the leader is too low to be detected by camera measurements probably due to increased conductivity resulting from repeated (relatively low amplitude) current pulses flowing via the lower channel section to ground (Visacro et al., 2017a) as the leader progresses upward. This is consistent with our UCL observation in Fig. 4a, where the section of the channel immediately above the tower is too dim to be imaged. However, our estimate of UCL speed of 4.6  $\times$  10<sup>5</sup> m/s from the frame shown in

Fig. 4a is primarily dependent upon our ability to detect the tip of UCL. The vicinity of the leader-tip is often the most luminous section of the channel from which luminosity pulses repeatedly travel backward along the channel in developing downward negative (e.g., Wang et al., 1999; Khounate et al., 2021) and positive (e.g., Kong et al., 2008; Wang and Takagi, 2011) leaders as well as upward positive leaders (e.g., Visacro et al., 2017b, see their Figs. 1 and 2). Additionally, each video camera frame in our data contains an integration of light over the relatively long exposure time of 98.46  $\mu$ s, which makes it more likely that the portions of the UCL with relatively long-lasting brightness (such as near the UCL tip) would be detected. In summary, it is very unlikely that the portion of the UCL detected in the frame in Fig. 4a is somehow the lower section of the UCL, while the upper section of the channel closer to the tip remained undetected. Also, the pixel resolution for our video camera measurement was 0.313 m/pixel, so the error per pixel in the estimated 2-D length and speed for the 46.1-m UCL-length was just 0.68%.

Our downward leader speed of  $1.45 \times 10^5$  m/s, derived from sequential video-camera frames during 100 µs prior to attachment, is similar to the expected average speed of a negative stepped leader in cloud-to-ground lightning (Rakov and Uman, 2003). Visacro et al.



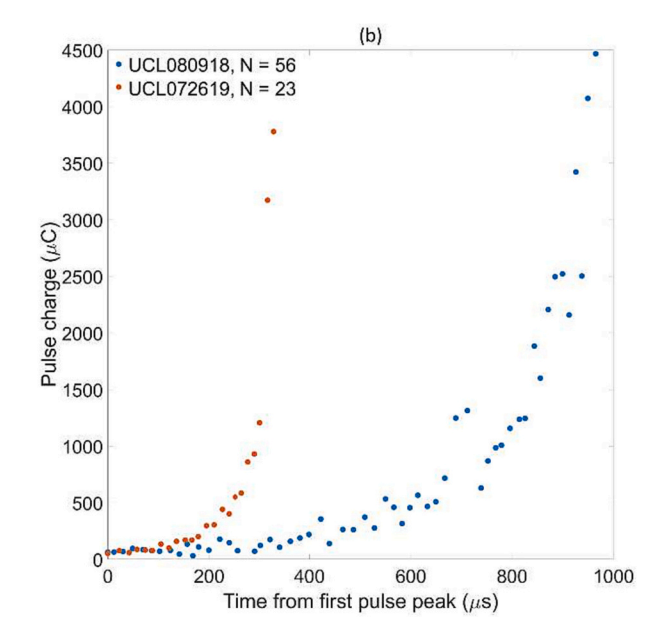


Fig. 7. (a) Histogram of the magnitude of pulse charge (charge injected by each UCL pulse) and (b) scatter plot showing pulse-charge magnitude versus time from first-pulse peak for 79 pulses in the two UCLs in our dataset, color-coded by flash ID. Note that these pulses injected positive charge into the UCLs, therefore, effectively transferring negative charge to ground. Statistics shown in (a) are sample size (N), median (Mdn), geometric mean (GM), arithmetic mean (AM), and standard deviation (SD). The corresponding maximum and minimum values are shown in Table 3.

(2017a), Saba et al. (2022), and Saba et al. (2023), respectively, reported average downward leader speeds of about  $2 \times 10^5$ ,  $1.2 \times 10^5$ , and  $2.9 \times 10^5$  m/s in Brazil. Note that, our downward leader speed is 4.6 times slower than the average speed of  $6.7 \times 10^5$  m/s reported by Tran and Rakov (2017). This faster average downward negative leader speed reported by Tran and Rakov versus in this study could be due to Tran and Rakov's observations being at lower altitude-ranges (about 30-120 m or so AGL for them versus at about 190 m in this study, see Fig. 4) with shorter upward leaders. The electric field environment ahead of the downward leader tip is expected to be more intense closer to groundlevel (e.g., Nag and Rakov, 2016). This hypothesis is supported by our observation of the LMA-derived average downward-leader vertical speed increase with decreasing altitude (between 5.5 and 2.75 km versus below 2.75 km) for the two stokes examined in this study (see Fig. 5). It is also consistent with Khounate et al. (2021)'s conclusion that leaderstep lengths and speeds are affected by the varying electric field environments at different altitudes above ground. Additionally, our leader vertical speeds were 2-2.7 times faster for the stroke with higher peakcurrent (3.6-6.3  $\times$  10<sup>5</sup> m/s for stroke 072619 with NLDN-estimated peak current of 98.5 kA versus 1.8–2.6  $\times$   $10^5$  m/s for stroke 080918 with 31.6-kA peak current). It is expected that higher return-stroke peak currents are associated with higher leader line-charge-densities (Khounate et al., 2021) that produce higher fields in which leaders may travel at faster speeds as they approach ground.

We computed an average line-charge-density of 0.5 mC/m for the full extent of the 109-m long UCL072619. Using measurements of electric field and modeling, Thomson et al. (1985) estimated the line charge densities for 10 negative downward stepped leaders near ground to be in the range of 0.7 to 32 mC/m, which is higher than our positively charged UCL's line-charge-density. Saba et al. (2023) reported line charge densities of 0.049 and 0.082 mC/m for a 40.2-m UUL and a 50.4-m UCL, respectively, from lightning rods 52 m AGL on a building in São Paulo City, Brazil associated with a 73-kA negative first return stroke. These line charge densities are about an order of magnitude lower than that reported by us and could be due to the peak current of our stroke being about 26% higher and our UCL-length being roughly twice that of theirs (due to our strike object being a tower with roughly twice the height of their building).

Our multi-channel current measurements (ranging from an RMS noise-floor of 0.64 A to saturation at 200 kA) allowed the detailed characterization of the UCL current leading to the rising portion of return stroke pulse for natural lightning. The onset of the slow front was marked with a relatively sharp change in the rate of current increase from the preceding UCL current. The beginning of this rapid change (see e.g., Fig. 2b) in current occurred within 1 µs of the saturation of our 600-A channel (Fig. 2a). This rapid increase in current is likely due to the formation of the common streamer zone as shown by the correlated current and ultra-high-speed video camera measurements of Plaisir et al. (2023). Note that we do not directly observe the common streamer zone in our video camera data in this study due to insufficient frame rate. Interestingly, Wang et al. (2014) observed a dramatic increase in luminosity in their "high-sensitivity" photodiode-array measurement channel centered at 34 m above ground followed, within a microsecond, by an increase in the luminosity in their "low-sensitivity" photodiodearray channel centered 27.8 m above ground; these channels were measuring light-intensity (with 6.2-m altitude resolution) associated with a stepped leader/first stroke sequence in an anomalous triggered lightning flash that struck a 10 m tall grounded, utility pole. Wang et al. (2014) observed slow front dE/dt pulses at the onset the luminosityincrease in the 34-m photodiode-array channel and linked it with the "start" of the return stroke; this luminosity increase could perhaps be viewed as being associated with the rapid increase in current at the end of the UCL leading to the slow front (as observed in this study). Using high-speed video observations and currents inferred from magnetic field measurements, Tran and Rakov (2017) associated the slow front portion of the current waveform (which reaches about one-half of the return stroke current peak) with two leaders extending toward each other inside the common streamer zone (which is consistent with the slow-frontbreakthrough-phase hypothesis of Nag et al., 2012). Note that, traditionally, the slow front current has been associated with the returnstroke (rather than pre-return-stroke) process. The "proper" onset of the return stroke (post-attachment) is marked by the beginning of the fast transition (Rakov and Tran, 2019; Nag et al., 2023; Plaisir et al., 2023).

#### 4.2. UCL-parameter inter-relationships and comparison with UULs

Fig. 8 shows the scatter plots of various parameters of the two UCLs in our dataset. Fig. 8(a), (c), and (e) show, respectively, the absolute background current amplitude, absolute background-to-peak pulseamplitude, and interpulse interval versus time from first-pulse peak. It appears that for about the first 70% of the UCL duration after the firstpulse peak the background current and pulse-amplitudes did not change remarkably, after which there was rapid increase of these parameters. For UCL080918, during the first 70% of its duration, the median background current and pulse-amplitudes were 4.3 and 26.9 A (N = 37), respectively; for the later 30% of its duration, the median values increased to 61.7 and 131.5 A (N = 19), respectively. For UCL072619, the median values increased from 2.5 and 45.2 A (N = 15), respectively, during the first 70% of its duration to 36.3 and 157.3 A (N = 8), respectively, during the later 30% of its duration. The interpulse intervals for UCL080918 and UCL072619 decreased from 18.3 (N = 36) and 15.9  $\mu$ s (N=14), respectively, during the first 70% of the UCL duration to 14.6 (N = 19) and 12.8  $\mu$ s (N = 8), respectively, for the later 30% of the UCL duration. From Fig. 8b we see that the background-topeak pulse amplitudes increased as the UCL background current increased. Generally speaking, interpulse intervals were shorter for pulses with larger peak amplitudes and also when the UCL background current was higher (see Fig. 8d and f, respectively). This is consistent with our observations that pulse amplitudes were larger, background current was higher, and interpulse intervals were shorter at later times during UCLs, which can be attributed to the intensification of the local electric field due to the approaching downward negative leader (Nag et al., 2021). Note that, these observations regarding the behavior of UCLs at early versus later times are similar to the behavior of UULs during their development phase reported by Nag et al. (2021). Also, since we expect that the impulsive characteristics of a UCL are dominantly affected by the electric field pulses (displacement current) associated with the downward negative leader stepping, we should note that interpulse intervals of cloud-to-ground negative stepped-leader electric field pulses are shorter and their amplitudes are larger at later stages of the downward leader as it approaches ground (see for example, Rakov

and Uman, 2003, pp. 132–135). Finally, the expected relationship between the UCL impulsive characteristics and downward leader stepping is supported by the high-speed video camera observations of Saba et al. (2023) who reported a UUL and UCL in a downward negative stroke alternately "respond to" different approaching downward leader branches; their UUL and UCL current pulsations time-synchronized as the tips of upward leaders and downward leader branches became more proximate about 100 µs prior to the return stroke.

The overall UCL currents increased to few kiloamperes at the end of the UCL stage and they reached about 10 kA or more at the end of the slow front stage. On the other hand, the UUL currents reached about ten to several hundred amperes prior to their collapse. Generally speaking, the waveform characteristics of the UCL-pulses in this study are somewhat similar to those reported for UUL-pulses by Nag et al. (2021) (see their Fig. 4) at the same tower. However, some key differences can be noted between UCL- and UUL-pulses in regard to their background-topeak pulse amplitudes and injected pulse-charge. The median background-to-peak pulse amplitude was 1.7 times larger (51.1 A versus 30.1 A) for UCL pulses than that for UUL pulses. Also, just prior to attachment, the background-to-peak pulse amplitudes were larger for UCL pulses (>300 A) than for UUL pulses (<300 A) just prior to their collapse. The median charge injected by UCL pulses was 1.9 times higher than that for UUL pulses reported by Nag et al. (297 versus 157  $\mu$ C). At later stages (just prior to the attachment processes between the upward and downward leaders), the UCL-pulses injected more charge per pulse (about 3000–4500  $\mu$ C per pulse) than that by UUL-pulses (<1200  $\mu$ C per pulse) prior to "collapse" of the UULs. These differences are likely due to the fact that, by definition, UCLs are more closely approached by a downward leader branch (to which they ultimately attach) than in the case of UULs (which do not attach to downward leaders).

Our two strokes had dramatically different peak currents and were preceded by UCL-currents with differing characteristics. For the 23 UCL-pulses in the 98.5-kA stroke 072619, the median pulse durations, risetimes, and interpulse intervals were shorter and the median background-to-peak pulse amplitudes higher than for those for the 56 UCL-pulses in the 31.6-kA stroke 080918. Interestingly, for both strokes the UCL-pulses exhibit similar maximum pulse-charge magnitudes (3.8 mC and

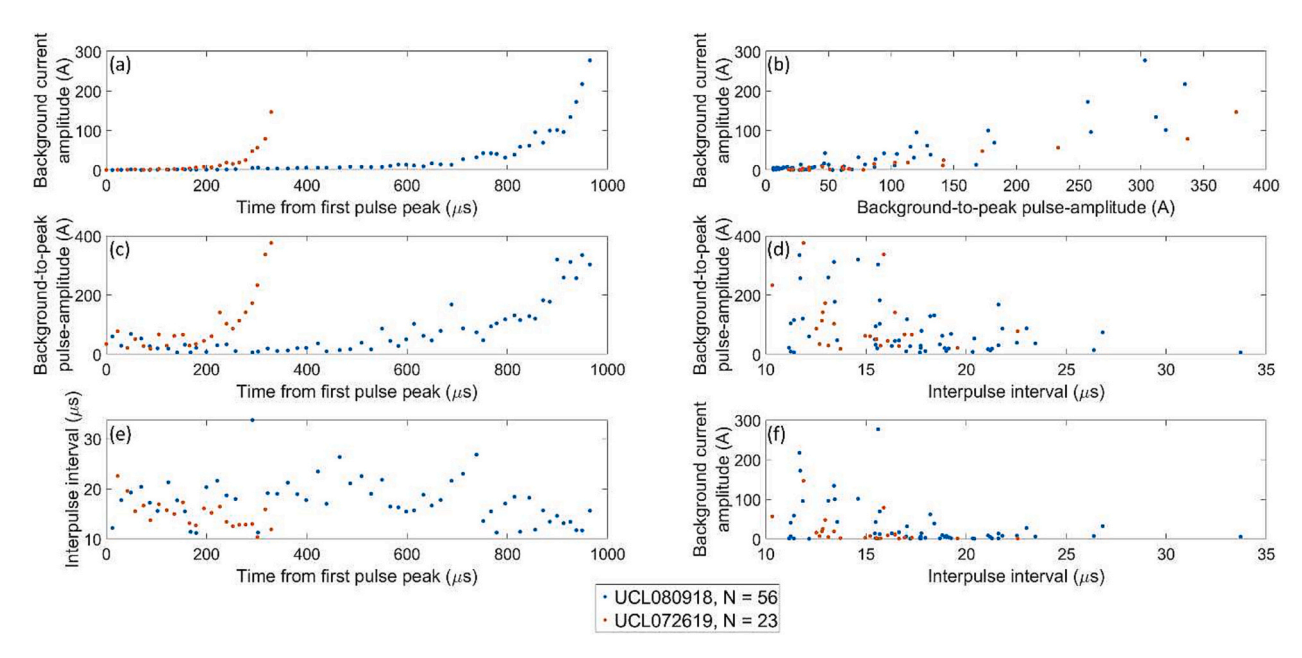


Fig. 8. Scatter plots of the (a) absolute background current amplitude versus time from first-pulse peak, (b) background current amplitude versus background-to-peak pulse-amplitude, (c) background-to-peak pulse-amplitude versus time from first-pulse peak, (d) background-to-peak pulse-amplitude versus interpulse interval, (e) interpulse interval versus time from first-pulse peak, and (f) background current amplitude versus interpulse interval for the two UCLs in our dataset, color-coded by flash ID (UCL080918 in blue and UCL072619 in brown). Note that the sample sizes in all parts are 56 and 23 for UCL080918 and UCL072619, respectively, except in (d) and (f) (in which interpulse interval is shown on the x-axes) where they are 55 and 22 for UCL080918 and UCL072619, respectively.

4.5 mC, respectively), but the UCL associated with the higher peakcurrent stroke (072619) produced these highest injected pulse-charge values about three times sooner (after the occurrence of the first pulse in the respective UCL, see Fig. 7b). This is likely due to the higher-peakcurrent stroke (which is expected to be associated with a higher-linecharge-density downward leader) having 2–2.7 times faster average downward leader vertical speeds (as discussed in Section 4.1).

Visacro et al. (2010) examined the characteristics of UCL current pulses in five negative first strokes (which they referred to as "pre-return-stroke pulses") that attached to the 60-m tall, insulated mast, on top of a mountain 1430 m above sea level, at the Morro do Cachimbo Station (MCS). They reported an AM pulse amplitude, interpulse interval, pulse duration, and risetime of 263 A, 61.9 µs, 7.5 µs, and 4 µs, respectively, for 104 UCL pulses. Their pulse amplitude is larger than our AM background-to-peak pulse amplitude of 86.8 A (see Fig. 6e) likely because we measured the peak pulse amplitudes from the background current-level rather than from the zero current-level, as apparently done by Visacro et al. (2010). Also, their AM interpulse interval is longer than our AM of 16.8 µs (see Fig. 6f) and their AM pulse duration is shorter than our AM of 11.7 µs (see Fig. 6a). Their AM risetime is similar to our AM background-to-peak risetime of 3.5 µs (see Fig. 6c). The exact reasons for the differences between the observations at the MCS and ours at the KSC IAT remain unknown; the various contributing factors can include the differences in the altitude of the measurement stations (at sea level for the KSC IAT versus 1430 m above sea level at the MCS), location of the current measurement on the towers (at the tower-top at the KSC IAT versus at the base of the 60-m mast at the MCS), local terrain (flat ground for the KSC IAT versus downward-sloping mountain-side at the MCS), and geographic locations (Titusville, Florida versus Belo Horizonte, Brazil). Interestingly, our interpulse intervals are similar to the AM and median interpulse intervals of 22.8 and 23 µs, respectively, reported by Saba et al. (2023) for 18 pulses in one UCL from a 52-m building in São Paulo City, Brazil. Note that the UCL-pulse median background-to-peak current amplitude reported by Saba et al. (102.5 A) was roughly two times higher than that in this study (51.1 A); the possible factors that could contribute to the difference in the UCL-pulse amplitudes are the UCL length (see Nag et al., 2021), distance of the UCL to the approaching downward leader, and the characteristics of the downward leader stepping which would determine the displacement current (proportional to the electric field derivative) between the downward leader and UCL. Finally, our median UCL pulse-charge magnitude (297 µC) is roughly an order of magnitude smaller than the estimated minimum charge involved in the formation of a downward leader step of 1-4 mC inferred by Krider et al. (1977).

# 5. Summary

We measured currents associated with two negative cloud-to-ground strokes attaching to the KSC IAT in August 2018 and July 2019. Our current measurements (ranging from an RMS noise-floor of 0.64 A to saturation at 200 kA) allowed us to examine in detail the characteristics of the current waveforms during the UCL stage as well as the rising portion of the following return-stroke pulses. The July 2019 stroke was also recorded at 10,000 frames per second using a high-speed video camera located 760 m from the KSC IAT. The NLDN-reported peak currents for the two strokes were -31.6 and -98.5 kA, respectively. During the UCL development phase, the current waveforms exhibited a monotonically (quasi-exponentially) increasing "background" current overlaid with 10-µs scale pulses with median amplitude of 51.1 A. The UCL current durations (time-interval between the inception of the UCLcurrent and the start of the slow front) for strokes 080918 and 072619 were 1039 and 449  $\mu s,$  respectively, during which 51.1 and 43 mC of negative charge, respectively, was effectively transferred to ground. The current increased in magnitude from zero to 1.5 kA and 3.6 kA at the end of the UCL stage for the two strokes, respectively. The slow fronts in the current waveforms occurred after the UCL-pulsations (at the end of the

UCL stage); the slow-front durations were 2.2 and 1.8 µs, respectively, for the two strokes. During the slow front, the current increased by 11.8 and 7 kA to reach amplitudes of 13.3 and 10.6 kA for the two strokes, respectively, which were 37 and 10.8% of the respective return-stroke peak current. The rapid increase in current (about 10 kA over roughly 2 µs) during the slow front is likely due to the formation of the common streamer zone as shown by the time-correlated current and ultra-highspeed video camera measurements of Plaisir et al. (2023). During the pre-attachment processes (UCL and slow front) the total negative charge effectively transferred to ground were 70.2 and 55 mC, for strokes 080918 and 072619, respectively. It is our perspective that the "proper" onset of the return stroke (post-attachment) is marked by the beginning of the fast transition; this is different than the traditional definition of the return stroke which includes both the slow front and fast transition portions of the return-stroke pulse as part of the post-attachment return stroke.

We computed an average line-charge-density of 0.5 mC/m for the 109-m long UCL072619. The average UCL 2-D speed was  $2.4 \times 10^5$  m/s, and it was observed to accelerate toward the downward leader prior to attachment. We observed that UCL pulse amplitudes were larger, background current was higher, and interpulse intervals were shorter at later times during UCLs, which can be attributed to the intensification of the local electric field due to the approaching downward negative leader. The median positive charge injected into the UCL (or negative charge transferred to ground) by UCL pulses was 297 μC. The median background-to-peak pulse amplitude was 1.7 larger and the median charge injected by pulses was 1.9 times higher for UCL pulses than those for UUL pulses at the same tower reported by Nag et al. (2021). These differences are likely due to the fact that, by definition, UCLs are more closely approached by a downward leader branch (to which they ultimately attach) than in the case of UULs (which do not attach to downward leaders). Finally, the UCL associated with the higher peak-current stroke produced the highest injected pulse-charge values about three times sooner (after the occurrence of the first pulse in the respective UCL). This is likely due to the higher-peak-current stroke (expected to be associated with a higher-line-charge-density downward leader) having 2-2.7 times faster average downward leader vertical speeds.

# CRediT authorship contribution statement

Amitabh Nag: Investigation, Methodology, Supervision, Formal analysis, Funding acquisition, Writing – original draft. Kenneth L. Cummins: Methodology, Investigation, Funding acquisition, Writing – review & editing. Mathieu N. Plaisir: Data curation, Investigation. Robert G. Brown: Investigation, Resources. Jennifer G. Wilson: Investigation, Resources. David E. Crawford: Investigation, Resources. R. Carl Noggle: Methodology, Investigation. Hamid K. Rassoul: Supervision, Funding acquisition, Writing – review & editing.

#### **Declaration of Competing Interest**

The authors declare that they have no known competing financial interests or personal relationships that could have appeared to influence the work reported in this paper.

# Data availability

Data will be made available on request.

#### Acknowledgements

The authors would like to acknowledge funding from the U.S. National Science Foundation Award 1934066 and U.S. Air Force contract FA252117P0079. We thank two anonymous reviewers for their thoughtful comments on the paper. Data used in this paper is available by contacting the first author (anag@fit.edu).

#### References

- Berger, K., Anderson, R.B., Kröninger, H., 1975. Parameters of lightning flashes. CIGRE Electra 41, 23–37
- Chen, L., Lyu, W., Ma, Y., Qi, Q., Wu, Zhang, Y., Yin, Q., Liu, H., Zhang, Y., Chen, S., Yan, X., Du, S., 2022. Return-stroke current measurement at the Canton Tower and preliminary analysis results. Electr. Power Syst. Res. 206 https://doi.org/10.1016/j.ensr.2022.107798
- CIGRE TB 549, 2013. Lightning parameters for engineering applications. In: WGC4.407, IISBN: 978–2–85873-244-9.
- Cooray, V., Montano, R., Rakov, V.A., 2004. A model to represent negative and positive lightning first strokes with connecting leaders. J. Electrost. 60, 97–109. https://doi. org/10.1016/j.elstat.2004.01.016.
- Fuchs, F., Landers, E.U., Schmid, R., Wiesinger, J., 1998. Lightning current and magnetic field parameters caused by lightning strikes to tall structures relating to interference of electronic systems. In: IEEE Transactions on Electromagnetic Compatibility, vol. 40, no. 4, pp. 444–451. Nov. 1998. https://doi.org/10.1109/15.736205.
- Hill, J.D., Mata, C.T., Nag, A., Roeder, W.P., 2016. Evaluation of the performance characteristics of MERLIN and NLDN based on two years of ground-truth data from Kennedy Space Center / Cape Canaveral Air Force Station, Florida. In: 24th International Lightning Detection Conference (ILDC). San Diego.
- Khounate, H., Nag, A., Plaisir, M.N., Imam, A.Y., Biagi, C.J., Rassoul, H.K., 2021. Insights on space leader characteristics and evolution in natural negative cloud-to-ground lightning. Geophys. Res. Lett. 48 https://doi.org/10.1029/2021GL093614 e2021GL093614.
- Kong, X., Qie, X., Zhao, Y., 2008. Characteristics of downward leader in a positive cloud-to-ground lightning flash observed by high-speed video camera and electric field changes. Geophys. Res. Lett. 35, L05816. https://doi.org/10.1029/2007GL032764.
- Krider, E.P., Weidman, C.D., Noggle, R.C., 1977. The electric fields produced by lightning stepped leaders. J. Geophys. Res. 82 (6), 951–960. https://doi.org/10.1029/ ic082i006p00951.
- Nag, A., Khounate, H., Cummins, K.L., Goldberg, D.J., Imam, A.Y., Plaisir, M.N., Rassoul, H.K., 2023. Parameters of the lightning attachment processes in a negative cloud-to-ground stroke observed on a microsecond timescale. Geophys. Res. Lett. 50 e2023GL104196. doi: 10.1029/2023GL104196.
- Nag, A., Murphy, M.J., Schulz, W., Cummins, K.L., 2015. Lightning locating systems: Insights on characteristics and validation techniques. Earth Space Sci. 2 https://doi. org/10.1002/2014EA000051.
- Nag, A., Rakov, V.A., 2016. A unified engineering model of the first stroke in downward negative lightning. J. Geophys. Res.-Atmos. 121 (5), 2188–2204. https://doi.org/ 10.1002/2015JD023777.
- Nag, A., Rakov, V.A., Tsalikis, D., Howard, J.S., Biagi, C.J., Hill, J.D., Uman, M.A., Jordan, D.M., 2012. Characteristics of the initial rising portion of near and far lightning return stroke electric field waveforms. Atmos. Res. 117 (2012), 71–77. https://doi.org/10.1016/j.atmosres.2011.08.012.
- Lu, W., Chen, L., Ma, Y., Rakov, V.A., Gao, Y., Zhang, Y., Yin, Q., Zhang, Y., 2013. Lightning attachment process involving connection of the downward negative leader to the lateral surface of the upward connecting leader. Geophys. Res. Lett. 40, 5531–5535. https://doi.org/10.1002/2013GL058060.
- Miki, T., Saito, M., Shindo, T., Ishii, M., 2019. Current Observation results of downward negative flashes at Tokyo Skytree from 2012 to 2018. IEEE Trans. Electromagn. Compat. 61 (3), 663–673. https://doi.org/10.1109/TEMC.2019.2910319.
- Nag, A., Cummins, K.L., Plaisir, M.N., Wilson, J.G., Crawford, D.E., Brown, R.G., et al., 2021. Inferences on upward leader characteristics from measured currents. Atmos. Res. 251 (December 2020) https://doi.org/10.1016/j.atmosres.2020.105420.
- Narita, T., Yamada, T., Mochizuki, A., Zaima, E., Ishii, M., 2000. Observation of current waveshapes of lightning strokes on transmission towers. IEEE Trans. Power Del. 15 (1), 429–435. Jan. 2000. https://doi.org/10.1109/61.847285.
- Plaisir, M.N., Nag, A., Cummins, K.L., Goldberg, D.J., Biagi, C.J., Brown, R.G., Rassoul, H.K., 2023. The lightning attachment processes observed on a submicrosecond-scale: Measurements of current and video. In: International Conference on Grounding & Lightning Physics and Effects, Belo Horizonte, Brazil -
- Qiu, Z., et al., 2019. 2019. Optical and current measurements of lightning attachment to the 356-m-high Shenzhen Meteorological Gradient Tower in southern coastal area of China. IEEE Access 7, 155372–155380. https://doi.org/10.1109/ ACCESS 2019.2944127
- Rakov, V.A., Tran, M.D., 2019. The breakthrough phase of lightning attachment process: from collision of opposite-polarity streamers to hot-channel connection. Electr. Power Syst. Res. 173, 122–134. https://doi.org/10.1016/j.epsr.2019.03.018.
- Rakov, V.A., Uman, M.A., 1998. Review and evaluation of lightning return stroke models including some aspects of their application. IEEE Trans. EMC 40 (4), 403–426. https://doi.org/10.1109/15.736202. Special Issue on Lightning.

- Rakov, V.A., Uman, M.A., 2003. Lightning Physics and Effects. Cambridge University Press.
- Roeder, W.P., Saul, J., 2017. The new mesoscale eastern range lightning information system. In: 18th Conference on Aviation Range and Aerospace Meteorology, American Meteorological Society Annual Meeting, Seattle, Washington.
- Saba, M.M.F., da Silva, D.R.R., Pantuso, J.G., da Silva, C.L., 2022. Close view of the lightning attachment process unveils the streamer zone fine structure. Geophys. Res. Lett. 49 https://doi.org/10.1029/2022GL101482 e2022GL101482.
- Saba, M.M.F., Lauria, P.B., Schumann, C., Silva, J.C.D.O., Mantovani, F.D.L., 2023. Upward leaders initiated from instrumented lightning rods during the approach of a downward leader in a cloud-to-ground flash. J. Geophys. Res.-Atmos. 128 https:// doi.org/10.1029/2022JD038082 e2022JD038082.
- Schulz, W., Nag, A., 2020. Lightning geolocation information for power system analyses. In: Lightning Interaction with Power Systems. The Institution of Engineering and Technology. ISBN: 978-1-83953-090-6.
- Takami, J., Okabe, S., 2007. Observational results of lightning current on transmission towers. IEEE Trans. Power Deliv. 22 (1), 547–556. https://doi.org/10.1109/ TPWRD.2006.883006.
- Thomson, E.M., Uman, M.A., Beasley, W.H., 1985. Speed and current for lightning stepped leaders near ground as determined from electric field records. J. Geophys. Res.-Atmos. 90 (D5), 8136–8142. https://doi.org/10.1029/JD090iD05p08136.
- Tran, M.D., Rakov, V.A., 2017. A study of the ground-attachment process in natural lightning with emphasis on its breakthrough phase. Sci. Rep. 7 (1), 1–13. https://doi. org/10.1038/s41598-017-14842-7.
- Visacro, S., Soares, A., Schroeder, M.A.O., Cherchiglia, L.C.L., de Sousa, V.J., 2004. Statistical analysis of lightning current parameters: measurements at Morro do Cachimbo station. J. Geophys. Res.-Atmos. 109 (D1) https://doi.org/10.1029/ 2003id003662.
- Visacro, S., Murta Vale, M.H., Correa, G., Teixeira, A., 2010. Early phase of lightning currents measured in a short tower associated with direct and nearby lightning strikes. J. Geophys. Res.-Atmos. 115 (16) https://doi.org/10.1029/2010JD014097.
- Visacro, S., Mesquita, C.R., De Conti, A., Silveira, F.H., 2012. Updated statistics of lightning currents measured at Morro do Cachimbo Station. Atmos. Res. 117, 55–63. https://doi.org/10.1016/j.atmosres.2011.07.010.
- Visacro, S., Guimaraes, M., Murta Vale, M.H., 2017a. Features of upward positive leaders initiated from towers in natural cloud-to-ground lightning based on simultaneous high-speed videos, measured currents, and electric fields. J. Geophys. Res.-Atmos. 122 (23), 12,786–12,800. https://doi.org/10.1002/2017JD027016.
- Visacro, S., Guimaraes, M., Murta Vale, M.H., 2017b. Striking distance determined from high-speed videos and measured currents in negative cloud-to-ground lightning. J. Geophys. Res.-Atmos. 122, 13,356–13,369. https://doi.org/10.1002/ 2017JD027354.
- Wang, D., Takagi, N., 2011. A downward positive leader that radiated optical pulses like a negative stepped leader. J. Geophys. Res. 116, D10205. https://doi.org/10.1029/ 2010/JD015391.
- Wang, D., Takagi, N., Watanabe, T., Rakov, V.A., Uman, M.A., 1999. Observed leader and return-stroke propagation characteristics in the bottom 400 m of a rockettriggered lightning channel. J. Geophys. Res. 104 (D12), 14369–14376. https://doi. org/10.1029/1999JD900201.
- Wang, D., Gamerota, W.R., Uman, M.A., Takagi, N., Hill, J.D., Pilkey, J., Ngin, T., Jordan, D.M., Mallick, S., Rakov, V.A., 2014. Lightning attachment processes of an "anomalous" triggered lightning discharge. J. Geophys. Res. Atmos. 119, 1524–1533. https://doi.org/10.1002/2013JD020787.
- Warner, T., 2010. Upward leader development from tall towers in response to downward stepped leaders. In: 30th International Conference on Lightning Protection. University of Cagliari, pp. 20–23.
- Warner, T.A., Cummins, K.L., Orville, R.E., 2012. Upward lightning observations from towers in Rapid City, South Dakota and comparison with National Lightning Detection Network data, 2004–2010. J. Geophys. Res. 117, D19109. https://doi.org/ 10.1029/2012.ID018346.
- Weidman, C.D., Krider, E.P., 1978. The fine structure of lightning return stroke waveforms. J. Geophys. Res. Oceans 83 (C12), 6239–6247. https://doi.org/ 10.1029/JC083iC12p06239.
- Weidman, C.D., Krider, E.P., 1980. Submicrosecond risetimes in lightning return-stroke fields. Geophys. Res. Lett. 7 (11), 955–958. https://doi.org/10.1029/ GL007i011n00955.
- Yuan, S., Jiang, R., Qie, X., Wang, D., Sun, Z., Liu, M., 2017. Characteristics of upward lightning on the Beijing 325 m meteorology tower and corresponding thunderstorm conditions. J. Geophys. Res.-Atmos. 122, 12,093–12,105. https://doi.org/10.1002/ 2017.ID027198
- Yuan, S., Qie, X., Jiang, R., Wang, D., Wang, Y., Wang, C., et al., 2021. In-cloud discharge of positive cloud-to-ground lightning and its influence on the initiation of towerinitiated upward lightning. J. Geophys. Res.-Atmos. 126 https://doi.org/10.1029/ 2021JD035600 e2021JD035600.